Chinese Chemical Letters 37 (2026) 112285

Contents lists available at ScienceDirect

Chinese Chemical Letters

journal homepage: www.elsevier.com/locate/cclet

Augmenting macropinocytosis enhances the apoptotic body-mediated tumor deep penetration of nanomedicines

Bin Wan[a,b,1], Qiu Wang[c,1], Xiwei Jiang[d,1], Xianlu Zhang[e,1], Xiaoyuan Fan[b], Fengxiang Liu[b], Shipeng Ning[a], Meiling Zhang[a], Dongyan Liang[a], Lianwen Qi[f], Zhonggui He[b,g], Yinglei Zhai[b], Kaiyuan Wang[b,g,h,*], Jin Sun[b,g,*], Wei Tang[a,*]

[a] Department of Breast Surgery, The Second Affiliated Hospital of Guangxi Medical University, Nanning 530000, China
[b] Department of Pharmaceutics, Wuya College of Innovation, Shenyang Pharmaceutical University, Shenyang 110016, China
[c] Department of Biomedical Engineering, College of Future Technology, Peking University, Beijing 100871, China
[d] School of Medical Devices, Shenyang Pharmaceutical University, Shenyang 110016, China
[e] Department of Urology, the First Hospital of China Medical University, Shenyang 110000, China
[f] School of Traditional Chinese Materia Medica, Shenyang Pharmaceutical University, Shenyang 110016, China
[g] Joint International Research Laboratory of Intelligent Drug Delivery Systems, Ministry of Education, Shenyang 110016, China
[h] Departments of Diagnostic Radiology, Surgery, Chemical and Biomolecular Engineering, and Biomedical Engineering, Yong Loo Lin School of Medicine and College of Design and Engineering, National University of Singapore, Singapore 119074, Singapore

ARTICLE INFO

Article history:
Received 14 August 2025
Revised 12 December 2025
Accepted 15 December 2025
Available online 15 December 2025

Keywords:
Cytomembrane nanovesicles
Apoptotic body
Macropinocytosis
Neighboring effect
Programmed drug penetration

ABSTRACT

Overcoming the penetration barrier of nanomedicines remains a paramount challenge in antitumor therapy. Apoptotic bodies (ApoBDs), which are naturally generated from apoptotic cells, can mediate a potent neighboring effect by transferring drug to neighboring tumor cells *via* macropinocytosis. To amplify this process, we developed a tumor microenvironment-responsive nanoplatform (named as AD-NVs@CPP) to selectively enhance chemokine (C-X-C motif) receptor 4 (CXCR4) receptor-stimulated macropinocytosis. This platform was constructed by co-encapsulating doxorubicin (DOX) and the hypoxia-activated prodrug AQ4N into homologous tumor cell membrane-derived nanovesicles (AD-NVs), followed by biomineralization of a calcium phosphate (CaP) shell that incorporated a CXCR4-targeting peptide (RFFESHAPAKPVSLSYR). The resultant AD-NVs@CPP exhibited a core-shell structure with a hydrodynamic diameter of ~180 nm and achieved a high peptide encapsulation efficiency of 81.6% ± 8.2%. The CaP shell demonstrated excellent pH-responsive dissolution, releasing ~50% of the peptide within 24 h at pH 6.5 (*vs.* negligible release at pH 7.4), which consequently promoted cellular uptake and enhanced cytotoxicity under acidic conditions *in vitro*. Additionally, AD-NVs@CPP-induced ApoBDs served as efficient drug reservoirs, delivering drugs to adjacent cells with an IC_{50} value of 0.98 μg/mL (in terms of protein concentration). *In vivo*, AD-NVs@CPP significantly prolonged the blood circulation time (increasing the half-life of DOX compared to the free drug solution) and improved tumor accumulation. Crucially, it enabled programmed drug penetration: AQ4N was selectively delivered into deep hypoxic tumor regions, mediating comprehensive tumor growth inhibition while maintaining a favorable safety profile. This work provides a robust strategy for achieving deep tumor penetration through the synergistic enhancement of macropinocytosis and the ApoBD-mediated neighboring effect.

© 2026 Published by Elsevier B.V. on behalf of Chinese Chemical Society and Institute of Materia Medica, Chinese Academy of Medical Sciences.

In the area of chemotherapy, the utilization of nanomedicines with a neighboring effect has emerged as a promising approach to enhance drug penetration and augment cytotoxicity in tumors [1–3]. Our previous investigations have revealed the pivotal contribution of apoptotic bodies (ApoBDs), a specific subclass of extracellular vesicles, in facilitating this phenomenon [4,5]. ApoBDs, which are typically released as blebs from apoptotic cells, encapsulate cytoplasmic components containing organelles and molecular cargos [6]. This unique packaging enables them to engage in interactions with neighboring cells. Consequently, ApoBDs effectively sequester the remaining drugs within apoptotic cells and subsequently transfer them to adjacent tumor cells, facilitating sequential intra-intercellular drug delivery and eliciting a robust neigh-

* Corresponding authors.
E-mail addresses: wangkaiyuan@hotmail.com (K. Wang), sunjin@syphu.edu.cn (J. Sun), tang_wei_gxmuch@163.com (W. Tang).
[1] These authors contributed equally to this work.

https://doi.org/10.1016/j.cclet.2025.112285
1001-8417/© 2026 Published by Elsevier B.V. on behalf of Chinese Chemical Society and Institute of Materia Medica, Chinese Academy of Medical Sciences.

boring effect. Furthermore, the neighboring tumor cells have the capacity to take up ApoBDs *via* the macropinocytosis pathway, enhancing the extensive intercellular penetration of drugs carried by ApoBDs [7].

Macropinocytosis, an actin-driven clathrin-independent endocytic pathway, plays a critical role in the metabolic adaptation of tumor cells. This process facilitates the uptake of extracellular proteins, providing essential amino acids for the rapid proliferation of cancer cells [8]. Moreover, macropinocytosis enables the internalization of protein-based drugs and exosomes within tumor cells [9]. The upregulation of chemokine (C-X-C motif) receptor 4 (CXCR4) has been observed in >23 different cancer types [10–12]. CXCR4 acts as a coreceptor for extracellular amino acids, oligoarginine cell-penetrating peptides, and other protein-based vesicles. Activation of CXCR4 efficiently triggers the macropinocytosis pathway, facilitating nutrient uptake by the cells [13,14]. Stromal cell-derived factor 1 (SDF1, C-X-C motif chemokine ligand 12 (CXCL12)) binds to the CXCR4 receptor and stimulates the macropinocytosis pathway [15]. Several mimetic peptides of CXCL12, such as RFFESH, KPVSLSYR, and RFFE-SHAPAKPVSLSYR, have been identified to activate CXCR4-mediated micropinocytosis [16]. Notably, RFFE-SHAPAKPVSLSYR exhibits the most potent effect in promoting CXCR4 receptor-stimulated micropinocytosis [17]. Thus, we hypothesized that RFFE-SHAPAKPVSLSYR, a mimic peptide of CXCL12, could enhance CXCR4 receptor-stimulated macropinocytosis, leading to improved internalization efficiency of ApoBDs by tumor cells. Furthermore, to address the potential issues of metabolism or absorption of mimic peptides during *in vivo* circulation, biocompatible materials responsive to the tumor microenvironment, such as calcium phosphate (CaP) and calcium carbonate, have been utilized for encapsulating the mimic peptide within nanoparticles. This strategy ensures the efficient binding of the encapsulated mimic peptide to the relevant receptors on CXCR4 and the activation of CXCR4 receptor-stimulated macropinocytosis, even during extended blood circulation [18–20]. Consequently, the development of a nanoplatform integrating the mimic peptides (RFFE-SHAPAKPVSLSYR) into a CaP shell to facilitate CXCR4 receptor-stimulated macropinocytosis represents a promising approach. This nanoplatform selectively enhances CXCR4 receptor-stimulated macropinocytosis at the tumor site, thereby improving the intracellular delivery efficiency of ApoBDs in tumor cells.

According to previous reports, the ApoBD-mediated neighboring effect has the potential to enhance the penetration efficiency of chemotherapy drugs in solid tumors and amplify therapeutic effects. However, the underlying mechanisms of this effect are not yet fully understood. Intracellular drugs consist of inactivated drugs tightly bound to the target site, active unbound drugs, and inactive prodrugs covalently linked to protective groups. Therefore, it is crucial to investigate the behavior of different drug states at each stage of ApoBD-mediated intercellular drug delivery to reveal the mechanisms. Previous studies have highlighted that the diffusion and range of the neighboring effect are inherently limited [21]. Consequently, monotherapy with a single drug is insufficient to continuously deliver active agents to the inner regions of solid tumors through this neighboring effect alone. This limitation leads to reduced cytotoxicity as penetration progresses, posing challenges in achieving deep penetration and complete tumor eradication. Hypoxia-activated prodrugs (HAPs) exhibit low or non-toxicity under normal physiological conditions but can be activated by highly expressed reductases in hypoxic tumor cells [22,23]. Furthermore, as penetration into the interior of the tumor, the oxygen level gradually decreases [24]. To address these challenges, we developed a nanocarrier to deliver both cytotoxic drugs and HAPs as active and inactive model drugs, respectively [25]. During the ApoBD-mediated intercellular drug delivery process, there is a continuous increase in the proportion of inactivated bound drugs

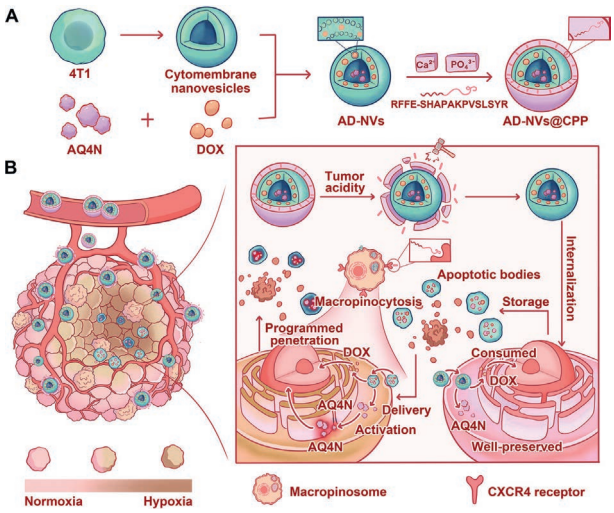


Fig. 1. Schematic diagram. (A) Construction of AD-NVs@CPP. (B) AD-NVs@CPP facilitates macropinocytosis in tumor cells and enhances selective drug delivery mediated by ApoBDs, enabling deep penetration of drugs into tumor tissues and completing tumor cell killing.

within the active drug prototype, accompanied by a gradual decrease in the proportion of active unbound drugs. In contrast, inactive HAPs are efficiently stored in ApoBDs and can be effectively transported between cells. By combining HAPs with conventional chemotherapy drugs, this approach overcomes the delivery barriers associated with the neighboring effect and enables the delivery of inactive prodrugs to the deep regions of tumors, thereby achieving programmed drug penetration.

Cell membrane nanovesicles (NVs) have emerged as highly promising targeting carriers for small molecule drug delivery [26–28]. These NVs offer unique advantages, including high biocompatibility and biodegradability, flexibility in encapsulating various bioactive molecules, and controllable sizes [29–31]. In addition, compared to autophagosomes and exosomes, extracellular microvesicles (EMVs) exhibit a simpler extraction process, higher encapsulation efficiency, and lower immunogenicity, making them advantageous for therapeutic cargo delivery [32–36]. In this study, we extracted homologous cell membrane NVs from murine breast cancer (4T1) cells *via* differential centrifugation to encapsulate and deliver two drugs with distinct spatial activities, doxorubicin (DOX) and the hypoxia-activated prodrug AQ4N. Concurrently, we engineered a core-shell nanoplatform (AD-NVs@CPP) by mineralizing dual-channel fluorescently labeled nanoparticles with CaP containing the peptide RFFE-SHAPAKPVSLSYR (Fig. 1A). The pH-responsive CaP shell dissolves rapidly in the tumor microenvironment, facilitating the targeted release of RFFE-SHAPAKPVSLSYR in the tumor region. This pH-dependent release selectively enhances macropinocytosis, exposing the nano-core for targeted tumor cells killing (Fig. 1B). DOX induces apoptosis in normoxic tumor regions, leading to the formation of ApoBDs. During this process, some DOX within ApoBDs becomes inactive due to binding to intracellular targets in tumor cells. Subsequently, the ratio of inactive bound DOX to active unbound DOX increases during intercellular transport. In contrast, AQ4N is effectively sequestered within ApoBDs, demonstrating high delivery efficiency. Through this programmed drug delivery process, sufficient AQ4N and small amounts of active DOX are delivered into the deep hypoxic regions of tumor cells in an ApoBD-mediated manner. Upon activation in the hypoxic environment, AQ4N exerts its cytotoxic effects. This ApoBD-based intercellular drug delivery achieves programmed drug penetration within tumors. Additionally, the RFFE-SHAPAKPVSLSYR peptide specifically promoted macropinocytosis, further enhancing

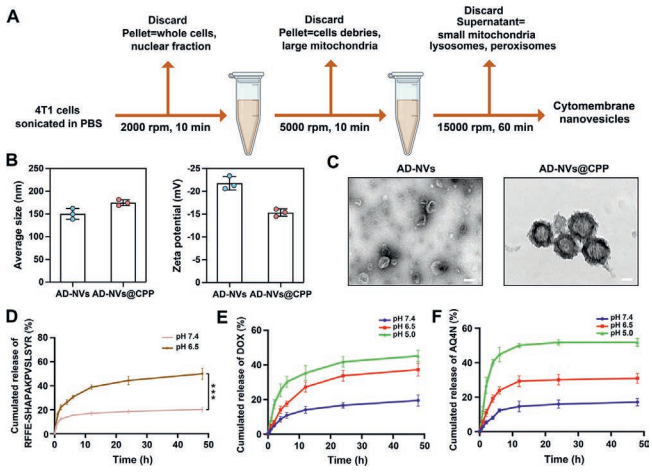


Fig. 2. Characterization of pH-responsive AD-NVs@CPP. (A) Extraction of cell membrane NVs by differential centrifugation. (B) Hydrodynamic sizes (volume mean) and zeta potentials of AD-NVs and AD-NVs@CPP measured by DLS. (C) TEM images of AD-NVs and AD-NVs@CPP. Scale bar: 100 nm. (D) RFFE-SHAPAKPVSLSYR release profiles of AD-NVs@CPP in release buffer at different pH values (6.5 and 7.4). Cumulative (E) DOX and (F) AQ4N release profiles of AD-NVs@CPP at different pH values (5.0, 6.5, and 7.4). Data are exhibited as the mean ± SD ($n = 3$). Statistical significance was calculated by two-tailed Student's *t*-test ($^{***}P < 0.001$).

penetration. In this study, we developed a customized nanoplatform and comprehensively evaluated its programmed tumor penetration and whole tumor-killing effects in the 4T1 breast tumor model.

Homologous cell membrane NVs were extracted from murine breast cancer cells (4T1) *via* differential centrifugation (Fig. 2A). AQ4N and DOX were co-encapsulated within the extracted NVs using an ultrasonic fragmentation method, forming the drug-loaded nanocore AD-NVs. By screening various drug mass ratios for encapsulation efficiency, an optimal fixed weight ratio of 1:1 for AQ4N and DOX was identified, yielding AD-NVs with ideal particle size and high drug encapsulation efficiency (Table S1 in Supporting information). To enhance this system, we employed a biomineralization strategy to modify the drug-loaded NVs with a CaP shell containing the peptide RFFE-SHAPAKPVSLSYR, forming AD-NVs@CPP. The encapsulation efficiency of RFFE-SHAPAKPVSLSYR, determined by bicinchoninic acid assay (BCA), was 81.6% ± 8.2%.

Dynamic light scattering (DLS) measurements showed that both the hydrodynamic diameter and zeta potential of AD-NVs@CPP increased compared to AD-NVs (Fig. 2B). Transmission electron microscopy (TEM) imaging revealed that the mineralized drug-loaded NVs transformed from a disc-like shape to a distinct core-shell nanosphere structure (Fig. 2C). We assessed the dissolution of the CaP shell under different pH conditions, including physiological (pH 7.4) and tumor microenvironment (pH 6.5), by measuring the release of Ca^{2+}. The results showed that approximately 80% of Ca^{2+} was released at pH 6.5 after 12 h, whereas only about 20% was released at pH 7.4 (Fig. S1A in Supporting information). Additionally, at pH 6.5, the size of the nanoparticles decreased from approximately 180 nm to ~150 nm as Ca^{2+} was released, corresponding to the size of AD-NVs (Fig. S1B in Supporting information). Further characterization of the AD-NVs@CPP formulation was performed using Fourier transform infrared spectroscopy (FTIR) spectroscopy. Results revealed distinct characteristic overlapping absorption peaks corresponding to both CaP and AD-NVs in the FTIR spectrum of AD-NVs@CPP (Fig. S2 in Supporting information), confirming the successful mineralization of CaP on the surface of AD-NVs. Furthermore, we investigated the release of the peptide under different pH conditions. The results indicated that at pH 6.5, about 50% of the peptide was released within 24 h due to the acid-responsive dissolution of the CaP shell, significantly higher than the release observed at pH 7.4 (Fig. 2D). The hydrodynamic particle size and polydispersity index (PDI) of AD-NVs@CPP remained largely unchanged following storage at 4 °C for 7 days and incubation in 10% fetal bovine serum (FBS) for 12 h, indicating excellent colloidal stability (Fig. S3 in Supporting information). These results indicated that AD-NVs@CPP exhibited excellent stability during *in vivo* circulation, effectively encapsulated the peptide, and released it in the tumor microenvironment. Additionally, we evaluated the release profiles of AQ4N and DOX from AD-NVs@CPP under different pH conditions. The results showed that only small amounts of DOX and AQ4N were released at neutral pH 7.4. However, under acidic conditions (pH 6.5 and 5.0), the release amount and rate of DOX and AQ4N significantly increased, with a more pronounced increase at pH 5.0 compared to pH 6.5 (Figs. 2E and F).

At this stage, we initially explored the primary pathway for AD-NVs uptake by 4T1 cells. Flow cytometry analysis revealed that macropinocytosis is the predominant internalization mechanism, with the process being energy-dependent (Fig. S4 in Supporting information). Internalization of ApoBDs by 4T1 cells is predominantly mediated by micropinocytosis. Quantitative analysis *via* flow cytometry revealed that approximately 40% of total ApoBD internalization occurs through this pathway (Fig. S5 in Supporting information). Subsequently, we employed confocal laser scanning microscopy (CLSM) to examine the fluorescence intensity of DOX and AQ4N, thereby elucidating the uptake of various formulations by 4T1 cells. Considering the specific affinity of homologous cell membrane NVs for similar cells and their widespread application in targeted drug delivery [37], we found that AD-NVs exhibited significantly enhanced cellular uptake efficiency compared to free drugs (Fig. 3A and Fig. S6A in Supporting information). Notably, quantitative fluorescence analysis by flow cytometry showed that under acidic conditions (pH 6.5), AD-NVs@CPP exhibited the highest cellular uptake efficiency (Fig. 3B and Fig. S6B in Supporting information). Compared to pH 7.4, AD-NVs@CPP exhibited an approximately 1.45-fold increase in micropinocytosis-mediated uptake at pH 6.5, where the acidic microenvironment synergistically enhanced macropinocytosis through CaP shell shedding and the release of macropinocytosis-promoting peptides (Fig. S7 in Supporting information). These findings elucidate the molecular mechanism underlying the enhanced cellular uptake of AD-NVs@CPP in acidic environments and provide a mechanistic rationale for optimizing their tumor-targeted delivery.

The cytotoxicity of the nanoparticles was evaluated under the normoxic and hypoxic conditions using the MTT assay. The observations revealed that DOX, a broad-spectrum anti-tumor chemotherapeutic agent, exhibited significant cytotoxicity under both normoxic and hypoxic conditions (half maximal inhibitory concentration (IC_{50}): 100.3 ng/mL) (Figs. 3C and D). AQ4N, a hypoxia-activated prodrug, showed very low cytotoxicity under normoxic conditions. In contrast, under hypoxic conditions, the cytotoxicity of the AQ4N group significantly increased due to the activation of AQ4N in the hypoxic environment. These findings highlighted the potential of the combined application of DOX and AQ4N for comprehensive tumor tissue destruction. Moreover, consistent with the cellular uptake results, AD-NVs@CPP exhibited stronger cytotoxicity at pH 6.5 compared to pH 7.4, effectively killing tumor cells under the normoxic and hypoxic conditions. Notably, the toxicity of AD-NVs was lower than that of the AQ4N+DOX mixture due to the sustained-release properties of the nanoparticles.

We isolated ApoBDs from cells treated with AD-NVs@CPP (pH 6.5) under normoxic conditions and examined the potential of ApoBDs as drug storage reservoirs. TEM revealed that the collected ApoBDs had a spherical structure with a diameter of approximately 1 μm (Fig. 3E), consistent with literature reports [38].

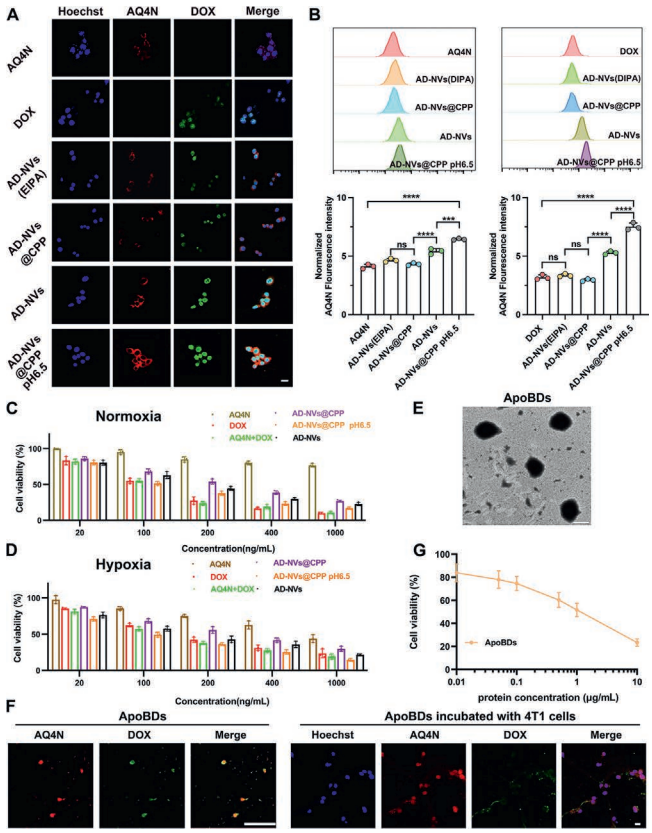


Fig. 3. *In vitro* cellular uptake, cytotoxicity, and characterization of AD-NVs@CPP - induced ApoBDs. (A) CLSM imaging of 4T1 cells incubated with AQ4N solution, DOX solution, AD-NVs (EIPA), AD-NVs and AD-NVs@CPP under the condition of different pH for 12 h. (B) Flow cytometry analysis of 4T1 cells incubated with AQ4N solution, DOX solution, AD-NVs (EIPA), AD-NVs and AD-NVs@CPP under the condition of different pH for 12 h. (C) Cell cytotoxicity of 4T1 cells treated with different formulations for 48 h under the condition of normoxia. (D) Cell cytotoxicity of 4T1 cells treated with different formulations for 48 h under the condition of hypoxia. (E) TEM image of ApoBDs. Scale bar: 1 μm. (F) CLSM images of ApoBDs and ApoBDs treated with 4T1 cells. Scale bar: 5 μm. (G) Cell cytotoxicity of ApoBDs against 4T1 cells after incubation for 48 h under the condition of normoxia ($n = 3$). Data are given as the mean ± SD. Statistical significance was calculated by two-tailed Student's *t*-test (ns, no significance. $^{***}P < 0.001$; $^{****}P < 0.0001$).

Additionally, Western blot (WB) analysis of ApoBDs confirmed their successful isolation, showing high levels of apoptotic markers, including cleaved caspase-3, and ApoBD-associated markers CD326 and CD44 (Fig. S8 in Supporting information). We assessed reactive oxygen species (ROS) generation in 4T1 cells following AD-NVs@CPP treatment using the ROS-specific fluorescent probe DCFH-DA. Fluorescence imaging and quantitative analyses revealed a significant increase in ROS fluorescence intensity in the AD-NVs@CPP-treated group compared to the AD-NVs-treated group. Notably, this ROS-elevating effect was markedly attenuated by the classic ROS scavenger NAC, indicating that AD-NVs@CPP specifically induces intracellular ROS accumulation (Fig. S9 in Supporting information). Most importantly, CLSM revealed distinct fluorescence signals of DOX and AQ4N within ApoBDs, and the drugs were effectively delivered to tumor cells (Fig. 3F). Furthermore, MTT cytotoxicity assays of drug-loaded ApoBDs showed that the drugs retained their ability to effectively kill tumor cells, with an IC_{50} value of 0.98 μg/mL for protein concentration (Fig. 3G). These findings were consistent with our previous research, further demonstrating the potential of ApoBDs as promising drug reservoirs in intercellular drug delivery processes.

At this stage, we co-incubated different formulations with 4T1 cells under normoxic conditions to generate drug-loaded ApoBDs. The drug-loaded ApoBDs were then extracted and co-incubated with 4T1 cells to construct models representing different stages of the drug delivery process and to explore the neighboring effect mechanisms mediated by ApoBDs (Fig. 4A). CLSM observations revealed that cells treated with AD-NVs and AD-NVs@CPP (pH 6.5) effectively delivered the drug to adjacent second well (ii-I) cells. Notably, the AD-NVs@CPP (pH 6.5) treatment group still exhibited significant AQ4N red fluorescence in the third well (iii-I) cells (Fig. 4B). Importantly, the green fluorescence of DOX in the second well (ii-I) cells diminished and was almost undetectable in the third well (iii-I) cells, while AQ4N red fluorescence remained prominent. Additionally, the fluorescence intensity of drugs in the first well (i-I) cells was stronger in the AD-NVs@CPP (pH 6.5) treatment group compared to the AD-NVs group (Fig. 4B). This result could be attributed to the release of peptides that promote macropinocytosis, enhancing drug uptake by the cells.

Subsequently, we quantified the drug content in the first well (i-I) cells, ApoBDs (i-ii), and second well (ii-I) cells, representing drug internalization, storage in ApoBDs, and transfer, respectively. AQ4N, a hypoxia-activated prodrug, lacks specific intracellular targets in normoxic cells and therefore remains mostly unbound with low toxicity in the first well (i-I) cells. During intercellular drug delivery, the proportion of inactive unbound AQ4N did not significantly change (Fig. 4C). In contrast, DOX, as a DNA topoisomerase inhibitor, forms DNA-DOX complexes [39], constituting 33 % of total DOX in the first well (i-I) cells. Interestingly, the ratio of inactive bound DOX to active unbound DOX significantly increased in ApoBDs (i-ii) and further increased in the second well (ii-I) cells (Fig. 4D). Moreover, the ratio of total AQ4N to total DOX gradually increased during the ApoBD-mediated programmed drug delivery process (Fig. 4E). These results demonstrated that DOX-induced ApoBDs can effectively store AQ4N and efficiently deliver it to other cells. Additionally, WB results showed significantly higher expression of apoptosis markers γH2AX and cleaved caspase-3 in cells (i-A) compared to cells (i-I) (Fig. 4F). Only a small amount of cytotoxic AQ4N was detected in cells (i-A) (Fig. 4G). CLSM observations of drug fluorescence distribution in drug-loaded ApoBDs (i-ii) and ApoBDs (ii-iii) indicated that the red fluorescence of AQ4N did not significantly diminish, whereas the green fluorescence of DOX markedly decreased (Fig. S10 in Supporting information). These findings further corroborate that the consumption of DOX is a primary factor inducing the formation of ApoBDs, and that ApoBDs can effectively carry sufficient amounts of unbound and inactive AQ4N to deliver to deep tumor cells, thus achieving programmed drug delivery at the tumor site.

Further analysis compared the state of drugs within ApoBDs generated by the AD-NVs group and the DOX and AQ4N mixture group. Despite the strong cytotoxicity of DOX solution under normoxic conditions to effectively kill tumor cells and stimulate the generation of more ApoBDs, these ApoBDs did not exhibit strong neighboring effects. In contrast, the nanomedicine formulations, leveraging their sustained-release characteristics, are capable of more efficiently preserving DOX in a free and unbound state (Fig. S11A in Supporting information). Cytotoxicity analysis of ApoBDs generated by the two treatment groups revealed that ApoBDs from the AD-NVs treatment group exhibited relatively stronger cytotoxicity compared to those from the mixture treatment group (Fig. S11B in Supporting information). These findings underscore the significant advantages of nanomedicines in promoting neighboring effects, attributable to its controlled drug release mechanism and protective role for drugs, reducing their consumption in single cells and thereby effectively enhancing neighboring effects and facilitating long-distance drug delivery.

We established an *in vitro* three-dimensional tumor spheroid model to investigate the effect of RFFE-SHAPAKPVSLSYR-induced CXCR4 receptor-stimulated macropinocytosis on programmable

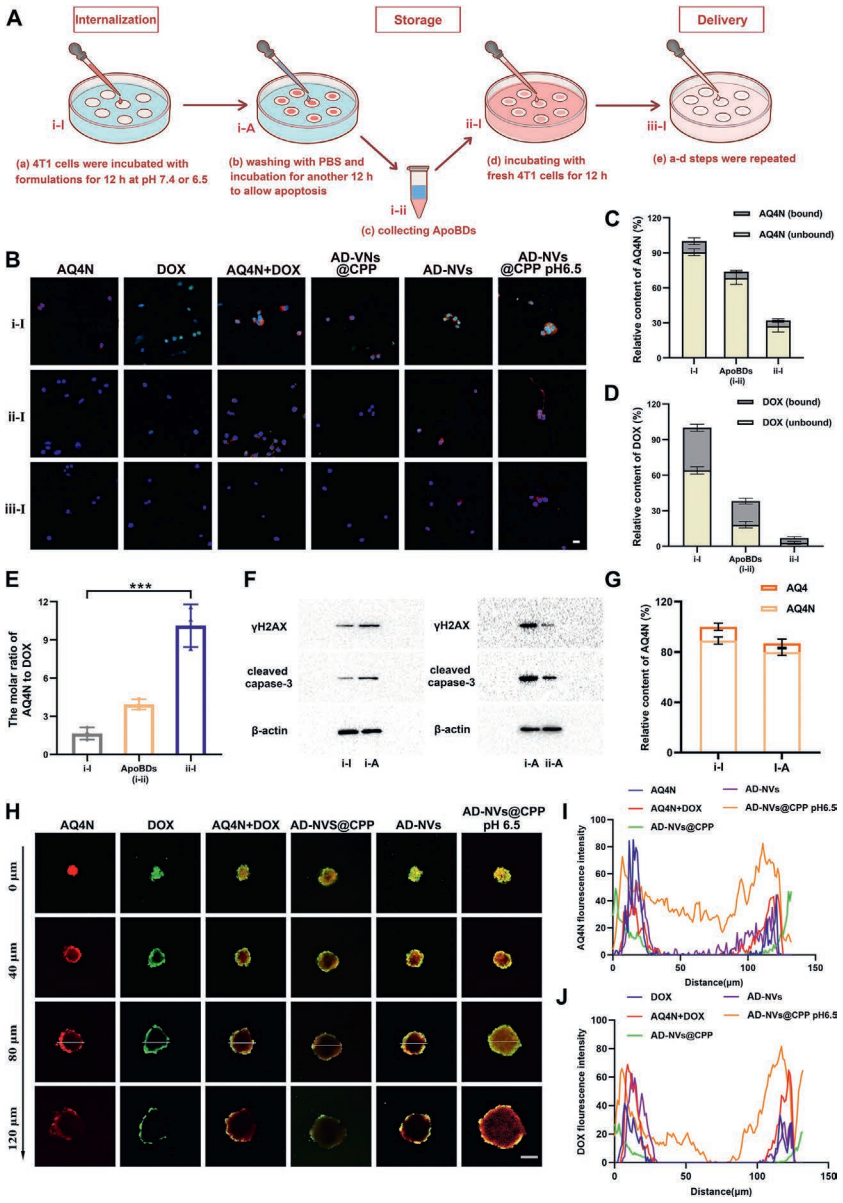


Fig. 4. Drug delivery and neighboring effect mechanisms mediated by ApoBDs in 4T1 cells. (A) Schematic illustration of co-incubation approach for investigating the ApoBDs-mediated programmed intercellular drug delivery. (B) Programmed intercellular drug delivery of different formulations observed by CLSM. Scale bar: 10 μm. (C) The relative proportion of bound/unbound AQ4N in cells (i-I), ApoBDs (i-ii), and cells (ii-I). (D) The relative proportion of bound/unbound DOX in cells (i-I), ApoBDs (i-ii), and cells (ii-I). (E) The molar ratio of total AQ4N and DOX in cells (i-I), ApoBDs (i-ii), and cells (ii-I). (F) WB assay of cleaved caspase-3 and γH2AX in cells (i-I), cells (i-A) and cells (ii -A). (G) The relative proportion of AQ4N and AQ4 in cells (i-I) and cells (i-A). (H) Z-stack images of 3D multicellular tumor spheroids. Scale bar: 100 μm. (I) AQ4N fluorescence quantitative analysis of multicellular tumor spheroids (MCTS) after treated with various formulations for 24 h. (J) DOX fluorescence quantitative analysis of MCTS after treated with various formulations for 24 h. Data are given as the mean ± SD ($n = 3$). Statistical significance was calculated by two-tailed Student's t-test ($^{***}P < 0.001$).

penetration. Our CLSM observations revealed that the combination therapy of both drugs exhibited superior penetration compared to the single drug solution group (Fig. 4H). Interestingly, AQ4N (red fluorescence) demonstrated better internal penetration than DOX (green fluorescence), reaching deeper regions within the tumor spheroid. Notably, the AD-NVs@CPP (pH 6.5) group exhibited the most pronounced programmable penetration effect, with noticeable red fluorescence of AQ4N even in the central region of the tumor spheroid. These findings collectively validate the feasibility and potential of achieving a "relay race"-like deep penetration through ApoBDs-mediated drug delivery. Furthermore, in the absence of the specific promotion of CXCR4 receptor-stimulated macropinocytosis by RFFE-SHAPAKPVSLSYR, AQ4N (red fluorescence) in other drug combination groups remained limited to the outer regions of the tumor spheroid and failed to reach the central area. Additionally, our quantitative analysis of drug penetration within the tumor spheroid corroborated with the CLSM observations (Figs. 4I and J). These results demonstrated that RFFE-SHAPAKPVSLSYR could specifically enhance macropinocytosis, promoting ApoBD-mediated programmable penetration, leading to comprehensive tumor growth inhibition.

To further delineate the *in vivo* fate of the AD-NVs@CPP, we performed a systematic pharmacokinetic analysis using Sprague-Dawley rats. All the animal protocols were performed in line with the Guidelines for the Care and Use of Laboratory Animals and approved by the Institutional Animal Care and Use Committee (IACUC) of Shenyang Pharmaceutical University (No. SYPU-IACUC–C2021–1–6–108). In the pharmacokinetic evaluation conducted *in vivo*, AD-NVs@CPP exhibited exceptional performance. As illustrated in Fig. 5A, the DOX solution was rapidly cleared from

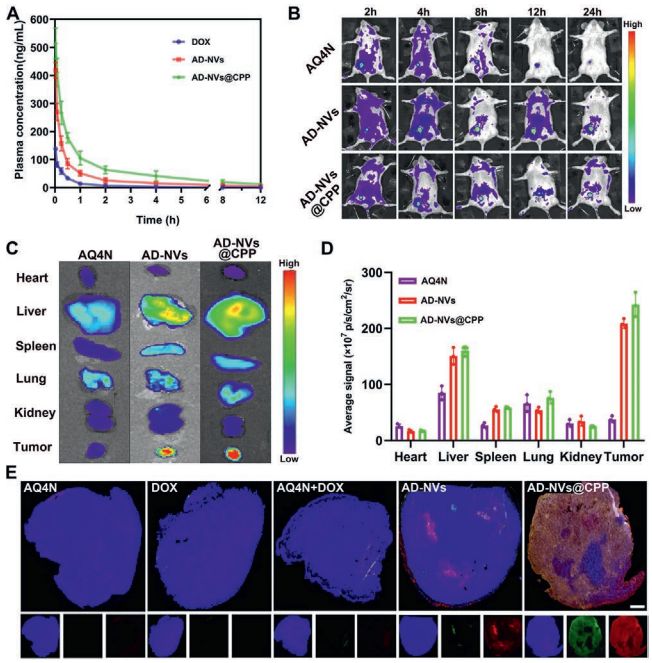


Fig. 5. Pharmacokinetics and biodistribution and *in vivo* penetration. (A) Concentration-time profiles of DOX in plasma after administration of different formulations. (B) *In vivo* distribution of AQ4N solution, AD-NVs, and AD-NVs@CPP in 4T1 tumor-bearing mice at 2, 4, 8, 12, and 24 h. (C) *Ex vivo* fluorescent images of AQ4N in heart, liver, spleen, lung, kidney and tumor at 24 h. (D) Semi-quantitative analysis of AQ4N in heart, liver, spleen, lung, kidney and tumor at 24 h. (E) CLSM images of tumor slices after administration with different formulations. Scale bar: 1 mm. 4′,6-Diamidino-2-phenylindole (DAPI), blue; DOX, green; AQ4N, red. Data are presented as the mean ± SD ($n = 3$). Statistical significance was calculated by two-tailed Student's *t*-test.

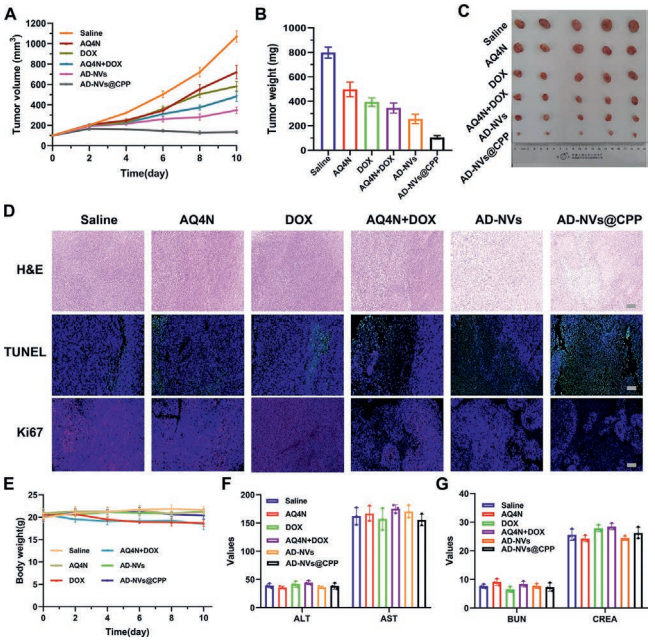


Fig. 6. *In vivo* antitumor activity and biosafety. (A) The tumor volume after administrated with different formulations ($n = 5$). (B) The tumor weights after administrated with different formulations ($n = 5$). (C) The tumor images after administrated with different formulations ($n = 5$). (D) H&E, TUNEL, and Ki 67 staining of tumors after injected with different formulations. Scale bar: 50 μm. (E) Body weight changes of bearing-tumor mice after administrated with different formulation. (F) The level of hepatic function in serum of bearing-tumor mice after administrated with different formulations ($n = 3$). (G) The level of renal function in serum of bearing-tumor mice after administrated with different formulations ($n = 3$). Data are presented as the mean ± SD. Statistical significance was calculated by two-tailed Student's *t*-test.

the bloodstream, with a half-life ($t_{1/2}$) of approximately 1.2 h. In contrast, AD-NVs significantly extended the half-life of the drug in the bloodstream, as detailed in Table S2 (Supporting information). Furthermore, compared to the DOX solution group, both AD-NVs and AD-NVs@CPP significantly increased the area under the concentration-time curve ($AUC_{0-24\,h}$), demonstrating that the cell membrane nanovesicles enhanced the stability of the drug in the blood and prolonged its circulation time. This extended circulation was advantageous for drug accumulation at the tumor site, thereby enhancing its antitumor efficacy. AD-NVs@CPP exhibited the most favorable pharmacokinetic properties *in vivo*. This superior performance could be attributed to the protective role of the CaP shell on its surface, which provides enhanced stability in the bloodstream. The CaP shell effectively shields the nanovesicles from shear forces in the blood, leading to a lower clearance rate [40–42].

We subsequently investigated the *in vivo* biodistribution of AD-NVs, AD-NVs@CPP, and AQ4N solution in a 4T1 tumor-bearing mouse model. As shown in Fig. 5B, the AQ4N solution was rapidly cleared from the body and did not exhibit specific organ accumulation. In contrast, both AD-NVs and AD-NVs@CPP displayed significant fluorescence accumulation in the tumor region, which increased with time, peaking at 12 h and remaining prominent even at 24 h post-injection. Furthermore, e*x vivo* fluorescence imaging of organs and tumor tissues at 24 h post-injection, coupled with semi-quantitative analysis, revealed substantial fluorescence accumulation in the tumor tissues for both AD-NVs and AD-NVs@CPP. These results were consistent with the pharmacokinetic analysis, highlighting the enhanced stability and tumor-targeting capabilities of the nanovesicle formulations (Figs. 5C and D).

Next, we examined the distribution of drug fluorescence in tumor tissues extracted from mice treated with different formulations after 24 h. Tumor sections were stained with DAPI and observed for drug fluorescence distribution. As shown in Fig. 5E, the AD-NVs@CPP group exhibited superior tumor penetration, with pronounced drug fluorescence observed even in the central regions of the tumors. This included the programmed penetration of both drugs, with the red fluorescence of AQ4N penetrating deeper into the tumor tissue compared to the green fluorescence of DOX. In contrast, AD-NVs, lacking the peptide that specifically promotes macropinocytosis in tumor cells, showed limited penetration into deeper tumor regions and primarily accumulated at the tumor periphery. The DOX and AQ4N mixed solution were unable to traverse multiple physiological barriers and was rapidly cleared from circulation, resulting in negligible drug fluorescence in the tumor tissue. Quantitative analysis of drug fluorescence intensity in tumor sections using ImageJ corroborated the microscopic observations, further confirming the distribution patterns observed (Fig. S12 in Supporting information). These results demonstrated that AD-NVs@CPP effectively prolong the circulation time and enhance the stability of the drug formulation *in vivo*. Moreover, AD-NVs@CPP could specifically target and accumulate in tumor tissues and, most importantly, exhibit excellent penetration into deeper tumor regions, ensuring efficient drug delivery to the inner areas of the tumor.

We conducted a comprehensive evaluation of the *in vivo* antitumor efficacy of AD-NVs@CPP in an orthotopic 4T1 tumor mouse model. Mice were randomly divided into six groups and received intravenous injections of saline, DOX solution, AQ4N solution, DOX+AQ4N mixed solution, AD-NVs, and AD-NVs@CPP. As shown in Figs. 6A–C, the saline group exhibited the fastest and most significant tumor volume growth. AD-NVs significantly inhibited tumor growth, demonstrating the superiority of cell membrane

NVs as drug delivery carriers. More importantly, compared to AD-NVs, AD-NVs@CPP exhibited markedly enhanced antitumor activity, effectively controlling tumor volume at approximately 100 mm^3 and essentially preventing further tumor growth. This outcome could be attributed to the RFFE-SHAPAKPVSLSYR peptide, encapsulated within the CaP shell, which is released responsively within the tumor microenvironment. This peptide specifically promoted macropinocytosis through stimulation of the CXCR4 receptor on tumor cells, thereby enhancing the programmed penetration of the combined DOX and AQ4N drugs into both normoxic and hypoxic regions of the tumor, achieving comprehensive tumor eradication. Furthermore, histological analyses of tumor sections from different treatment groups, including hematoxylin and eosin (H&E) staining, Ki67 staining, and terminal deoxynucleotidyl transferase-mediated dUTP nick-end labeling (TUNEL) staining, revealed that AD-NVs@CPP effectively induced tumor cell apoptosis and significantly reduced tumor cell proliferation. These results further demonstrated the therapeutic superiority of AD-NVs@CPP in tumor treatment (Fig. 6D). Additionally, the body weight changes of mice in different treatment groups were recorded (Fig. 6E). Mice in the AD-NVs@CPP treatment group maintained stable body weight, whereas those treated with DOX and the mixed solution exhibited significant weight loss, likely due to the known cardiotoxicity of DOX, particularly at cumulative doses, which poses a chronic toxicity risk to the heart [43–45]. Moreover, liver and kidney function markers, as well as inflammatory cytokines levels, in the AD-NVs@CPP group showed no significant differences compared with the saline-treated control group (Figs. 6F and G, Fig. S13 in Supporting information), indicating that AD-NVs@CPP did not adversely affect major organ functions.

In summary, we have successfully developed a novel biomineralized cell membrane nanovesicle (AD-NVs@CPP) that can achieve programmed deep penetration of drugs within tumor tissues through an ApoBD-mediated mechanism. We have focused on the neighbor effect of ApoBDs and the key factors that influence their drug delivery efficiency between cells. Additionally, we have evaluated the impact of macropinocytosis on deep tumor penetration mediated by ApoBDs. The principal findings of our study are summarized as follows. We extracted cell membrane vesicles from 4T1 cells and combined them with the broad-spectrum chemotherapeutic drug DOX and the hypoxia-activated prodrug AQ4N to construct a nano-core (AD-NVs). The AD-NVs were subsequently mineralized with a CaP shell, which was functionalized with a peptide (RFFE-SHAPAKPVSLSYR) that specifically binds to CXCR4 receptors on tumor cells and promotes macropinocytosis. This design enables the AD-NVs@CPP to selectively dissolve the CaP shell in the acidic tumor microenvironment, thereby releasing the peptide and the AD-NVs. In the mildly acidic tumor microenvironment, the CaP shell of AD-NVs@CPP specifically dissolves, exposing the intrinsic nano-core, thereby achieving targeted action and high cellular uptake by homologous tumor cells. As a result, AD-NVs@CPP can effectively eliminate tumor cells in both normoxic and hypoxic regions. The combined application of DOX and AQ4N induces the formation of ApoBDs containing these drugs, which through the neighbor effect, continue to affect surrounding tumor cells, achieving a programmed cytotoxic effect. As a promising drug carrier, ApoBDs can effectively carry and deliver drugs between cells. During this process, DOX is continuously consumed, inducing apoptosis in tumor cells and generating drug-loaded ApoBDs. The proportion of bound DOX increases, while AQ4N remains in a free state within normoxic tumor regions. AQ4N is then transported by ApoBDs to deep hypoxic tumor regions, where it is activated to exert cytotoxic effects on tumor cells, thereby achieving a programmed drug delivery within the tumor tissue. This programmed delivery strategy enhances therapeutic efficacy by ensuring effective distribution and utilization of drugs in the tumor microenvironment. The RFFE-SHAPAKPVSLSYR peptide in AD-NVs@CPP specifically promotes macropinocytosis in tumor cells, effectively enhancing their uptake of ApoBDs. This approach enables drugs to be delivered through an ApoBD-mediated neighbor effect to deep tumor regions, thereby achieving comprehensive eradication of tumor tissues. AD-NVs@CPP significantly extend the circulation time of drugs in the bloodstream, enabling their specific accumulation in tumor tissues and facilitating deep penetration. During the programmed drug penetration process, AQ4N penetrates deeper into tumor tissues compared to DOX. AD-NVs@CPP exhibit almost complete inhibition of tumor growth without significant systemic toxicity, demonstrating excellent antitumor activity and *in vivo* biosafety. Collectively, these findings demonstrate that AD-NVs@CPP provide a robust platform for targeted, deep tumor penetration and effective drug delivery, offering significant potential for improved cancer treatment strategies.

Declaration of competing interest

The authors declare that they have no known competing financial interests or personal relationships that could have appeared to influence the work reported in this paper.

CRediT authorship contribution statement

Bin Wan: Writing – review & editing, Writing – original draft, Visualization, Validation, Software, Project administration, Methodology, Investigation, Formal analysis, Data curation, Conceptualization. **Qiu Wang:** Writing – review & editing, Writing – original draft, Software, Project administration, Methodology, Funding acquisition, Formal analysis, Data curation. **Xiwei Jiang:** Writing – original draft, Resources, Methodology, Investigation, Data curation. **Xianlu Zhang:** Writing – review & editing, Writing – original draft, Project administration, Methodology. **Xiaoyuan Fan:** Software, Resources. **Fengxiang Liu:** Visualization, Validation. **Shipeng Ning:** Software, Methodology. **Meiling Zhang:** Formal analysis, Data curation. **Dongyan Liang:** Supervision. **Lianwen Qi:** Project administration. **Zhonggui He:** Investigation, Formal analysis. **Yinglei Zhai:** Visualization, Investigation. **Kaiyuan Wang:** Writing – review & editing, Writing – original draft, Visualization, Methodology, Funding acquisition, Formal analysis, Data curation. **Jin Sun:** Funding acquisition, Conceptualization. **Wei Tang:** Writing – review & editing, Writing – original draft, Visualization, Methodology, Funding acquisition, Formal analysis, Data curation.

Acknowledgments

We are grateful for the financial support from National Key R&D Program of China (No. 2022YFE0111600), National Natural Science Foundation of China (No. 82273874), Liaoning Province Applied Basic Research Program (No. 2025JH2/101330178), Liaoning Revitalization Talents Program (No. XLYC22202019), Postdoctoral Fellowship Program of China Postdoctoral Science Foundation (No. GZC20240050).

Supplementary materials

Supplementary material associated with this article can be found, in the online version, at doi:10.1016/j.cclet.2025.112285.

References

[1] C. Wang, S. Chen, Y. Wang, et al., Adv. Mater. 30 (2018) 1706407.
[2] S. Guo, Y. Wang, L. Miao, et al., ACS Nano 7 (2013) 9896–9904.
[3] J. Jiang, X. Cui, Y. Huang, et al., Nano Biomed. Eng. 16 (2024) 152–187.
[4] C. Ju, R. Mo, J. Xue, et al., Angew. Chem. 126 (2014) 6367–6372.
[5] D. Zhao, W. Tao, S. Li, et al., Sci. Adv. 7 (2021) eabg0880.

[6] C.D. Gregory, M.P. Rimmer, J. Pathol. 260 (2023) 592–608.
[7] X. Shen, D. Pan, Q. Gong, et al., Bioact. Mater. 32 (2023) 445–472.
[8] W. Palm, Philos. Trans. R. Soc. B: Biol. Sci. 374 (2019) 20180285.
[9] A.S. Desai, M.R. Hunter, A.N. Kapustin, Philos. Trans. R. Soc. B: Biol. Sci. 374 (2019) 20180156.
[10] A.M. Fulton, Chemokine receptors in cancer, in: B. Furusato, J.S. Rhim (Eds.), Introduction to the CXCR4 and Cancer, Humana Press, Inc., New Jersey, 2009, pp. 31–45.
[11] Z. Wang, Y. Ma, X. Yu, et al., Adv. Funct. Mater. 28 (2018) 1800732.
[12] H. Guo, Y. Ge, X. Li, et al., Signal Transduc. Target. Ther. 2 (2017) 17033.
[13] C. Yang, F. Zhang, F. Chen, et al., Adv. Healthc. Mater. 12 (2023) 2202064.
[14] L. Sun, X. Luo, C. Zhou, et al., Chin. Chem. Lett. 35 (2024) 108803.
[15] E.B. Cepeda, T. Dediulia, J. Fernando, et al., Biochim. Biophys. Acta 1853 (2015) 1205–1218.
[16] G. Jiang, H. Chen, J. Huang, et al., Adv. Sci. 7 (2020) 1903290.
[17] T.R.M. Filippo, L.T. Galindo, G.F. Barnabe, et al., Stem Cell Res. 41 (2020) 101631.
[18] K. Wang, X. Zhang, H. Ye, et al., Nat. Commun. 14 (2023) 6748.
[19] L. Ribovski, B. Joshi, J. Gao, et al., Extr. Vesicles Circ. Nucleic Acids 4 (2023) 283–305.
[20] G. Tanaka, I. Nakase, Y. Fukuda, et al., Chem. Biol. 19 (2012) 1437–1446.
[21] A. Sharma, J.F. Arambula, S. Koo, et al., Chem. Soc. Rev. 48 (2019) 771–813.
[22] Y. Li, L. Zhao, X.F. Li, Front. Oncol. 11 (2021) 700407.
[23] U.M. Kumar, U. Kumar, A.K. Singh, Nano Biomed. Eng. 14 (2022) 38–52.
[24] Y. Wang, S. Luo, Y. Wu, et al., ACS Nano 14 (2020) 17046–17062.
[25] S. Luo, C. Liang, Q. Zhang, et al., Chin. Chem. Lett. 34 (2023) 107666.
[26] D. Gupta, O.P.B. Wiklander, M.J.A. Wood, et al., Extr. Vesicles Circ. Nucleic Acids 4 (2023) 170–190.
[27] Y. He, K. Wang, Y. Lu, et al., Nano Lett. 22 (2022) 1415–1424.
[28] F. Sun, S. Ning, X. Fan, et al., Nano Today 61 (2025) 102604.
[29] X. Wang, I.M. Lei, B. Li, et al., Chin. Chem. Lett. 37 (2026) 110990.
[30] S. Hu, R. Hao, Z. Yu, et al., Chin. Chem. Lett. 35 (2024) 108534.
[31] X. Wang, S. Ning, W. Tao, et al., Nano Today 56 (2024) 102311.
[32] G. Huang, W. Zheng, Y. Zhou, et al., Acta Pharm. Sin. B 14 (2024) 3855–3875.
[33] S. Sheng, X. Yu, G. Xing, et al., Adv. Funct. Mater. 33 (2023) 2212118.
[34] Y. Yu, T. Li, M. Ou, et al., J. Control. Release 365 (2024) 469–479.
[35] J. Zhang, J. Guo, L. Wang, et al., J. Control. Release 376 (2024) 369–381.
[36] X. Wang, W. Chen, W. Zeng, et al., Acta Pharm. Sin. B 15 (2025) 3460–3486.
[37] M. Sun, J. Yang, Y. Fan, et al., Adv. Sci. 10 (2023) 2303617.
[38] R.J.C. Bose, N. Tharmalingam, F.J. Garcia Marques, et al., ACS Nano 14 (2020) 5818–5835.
[39] C. Carvalho, R.X. Santos, S. Cardoso, et al., Curr. Med. Chem. 16 (2009) 3267–3285.
[40] V. Sokolova, M. Epple, Chemistry 27 (2021) 7471–7488.
[41] S. Qing, C. Lyu, L. Zhu, et al., Adv. Mater. 32 (2020) 2002085.
[42] R. Khalifehzadeh, H. Arami, Adv. Colloid Interface Sci. 279 (2020) 102157.
[43] A. Pugazhendhi, T.N.J.I. Edison, B.K. Velmurugan, et al., Life Sci. 200 (2018) 26–30.
[44] A. Varela-López, M. Battino, M.D. Navarro-Hortal, et al., Food Chem. Toxicol. 134 (2019) 110834.
[45] G. Toffoli, M. Hadla, G. Corona, et al., Nanomedicine 10 (2015) 2963–2971.